CLAS-NOTE 2002-018

Transferred Polarization in $K^+\Lambda$ Electroproduction – Systematic Uncertainty Analysis for E99-006

Daniel S. Carman
Ohio University, Athens, OH 45701

October 31, 2002

Abstract

In this document I detail the systematic uncertainty analysis that was carried out as part of E99-006 in the measurement of the transferred polarization in $K^+\Lambda$ electroproduction. Each of the individual checks performed and the estimated uncertainty are described, along with the final systematic uncertainty quoted for the measurement. The information in this CLAS-Note has been extracted from the full E99-006 Analysis Document.

E99-006 Systematic Uncertainty Analysis

The purpose of this document is to describe in detail the procedures used for the determination of the systematic uncertainties assigned to the double-polarization observables in $K^+\Lambda$ electroproduction using the E1C data. These measurements are part of CLAS experiment E99-006 [1] that was designed to measure polarization observables in the $\vec{e}p \to e'K^+\vec{\Lambda}$ reaction at 2.5 and 4 GeV using the CLAS spectrometer in HALL B. The large acceptance of CLAS enabled us to detect the scattered electron, the electro-produced kaon, and the proton from the mesonic decay of the Λ hyperon over a range of Q^2 from 0.4 to 2.7 $(\mathrm{GeV/c})^2$ and W from 1.6 to 2.4 GeV, while spanning the full center-of-mass angular range for the kaon. The information in this CLAS-Note has been extracted from the full E99-006 Analysis Document [2].

CLAS completed its first polarized electron beam run on a hydrogen target in the period from January through April 1999. Data were acquired at beam energies of 2.567 GeV (I/I_{max} = 40%, 60%) and ≈4 GeV (specifically 4.056, 4.247, 4.462 GeV) (I/I_{max} = 60%, 90%). The CLAS data set for the 1999 e1 run (E1C) represents a sizeable fraction of the total expected $e+p$ data set (≈25%). As such, it provides us with an opportunity to study the physics of hyperon production with a statistical accuracy not possible with the CLAS E1A (Dec 1997) or E1B (Jan - Mar 1998) data sets. During E1C running, the CLAS readout was triggered by a coincidence between a Cerenkov counter and a forward calorimeter detector in a given sector (no second level trigger). During much of the E1C run period, the incident electron beam was longitudinally polarized to an average value of 67%. This value was determined from several HALL B Møller polarimeter runs spaced throughout the run period.

In this document we examine the sources of systematic uncertainty that effect the extracted polarization observables. The full details of the analysis are contained in the E99-006 Analysis Document [2]. The contributions to the total systematic uncertainty belong to one of four general categories:

- Polarization Extraction
- Acceptance Function
- Beam Related Factors
- Background Contributions

Each of these areas are discussed in the subsections that follow. The final systematic error compilation for this measurement is given in Table 3. In addition to the discussion of the above categories, additional studies to explore the systematics are included in Section 7.

1 Error Estimation

Both the 2.567 GeV and the 4 GeV data sets for this analysis are plagued by low statistics for the final state of interest. Thus unambiguous assignment of a systematic uncertainty for each identified source is not a straightforward procedure. We are always faced with a strong coupling between systematic effects and statistics. In some cases this has caused us to assign an uncertainty that may be too large. In the end, however, the statistical uncertainties outweigh the systematic uncertainties in all cases. Another important effect that we are faced

with when fitting the asymmetry distributions is that there is a clear statistical threshold below where the results of the polarization fits are totally unreliable. We have been careful to account for the problem fits in our analysis.

The procedure used to assign a systematic uncertainty to each source studied is to compare the polarization analysis results for all bins in Q^2, W, and $\cos\theta^*_K$ with the nominal analysis cuts in place and the modified cuts in place focussing on the polarization axes P'_ℓ and P'_t. A measure of the systematic uncertainty is the average difference between the polarizations extracted. For this analysis, our definition of the average polarization difference is given by:

$$\langle P \rangle = \sqrt{\frac{\sum_{i=1}^{n} \frac{[P_i^{nom} - P_i^{alt}]^2}{(\delta P_i)^2}}{\sum_{i=1}^{n} \frac{1}{(\delta P_i)^2}}}, \tag{1}$$

$$(\delta P_i)^2 = (\delta P_i^{nom})^2 + (\delta P_i^{alt})^2. \tag{2}$$

Here the sum runs over the n data points in a given data set, P_i^{nom} is the polarization of the i^{th} point of the data set with the nominal cuts in place, and P_i^{alt} is the polarization of the i^{th} point of the data with the altered cuts in place. The error weighting for a given polarization difference is given by the sum of the squares of the polarization uncertainty for the nominal polarization data points and the altered cut polarization data points.

In order to account for polarization fits where the fit results are unreliable, we enforce an upper limit on the polarization uncertainty of points in the calculation of $\langle P \rangle$. The value of the uncertainty cut-off depends on how the data is sorted and which kinematic variables are being summed over. The cut-offs are listed in Table 1 below.

Binning Variables	δP Cut Off
Q^2, W, $\cos\theta^*_K$	0.30
W, $\cos\theta^*_K$	0.25
W	0.20

Table 1: Upper limits on the polarization uncertainty for inclusion in the $\langle P \rangle$ calculation. The first column indicates the kinematic variables into which the data is binned.

In order to provide a crude check of our procedure, throughout this section we also compare our assigned systematic uncertainties to the RMS width of the polarization difference distribution. This width will certainly overestimate the systematic uncertainty, but at least provides one (upper) bound.

2 Polarization Extraction

The polarization has been extracted using two different analysis approaches. The nominal technique employs an asymmetry method in which the difference divided by the sum of the acceptance-corrected helicity-gated yields is used to extract the hyperon polarization,

$$A = \frac{\sigma^+ - \sigma^-}{\sigma^+ + \sigma^-} = \frac{\alpha P_b P'_\Lambda \cos\theta_p^{RF}}{1 + \alpha P^0_\Lambda \cos\theta_p^{RF}}. \tag{3}$$

In performing the integration over all relative Φ angles, the asymmetry becomes:

$$A = \alpha P_b P'_\Lambda \cos\theta_p^{RF}. \tag{4}$$

An alternative approach is to extract the polarization from the ratio of the acceptance-corrected helicity-gated yields via the so-called ratio approach:

$$R = \frac{\sigma^+}{\sigma^-} = \frac{1 + \alpha P_b P'_\Lambda \cos\theta_p^{RF}}{1 - \alpha P_b P'_\Lambda \cos\theta_p^{RF}}. \tag{5}$$

Representative fits are shown in Fig. 1. A comparison of the polarization results with the nominal asymmetry extraction vs. the ratio extraction is shown in Fig. 2. The assigned systematic uncertainty for the choice of extraction function is based on the average polarization difference between the two techniques of 0.013. The same uncertainty has been found for both the 2.567 GeV and the 4 GeV data sets. Fig. 3(left) shows the distribution of the polarization differences between the asymmetry approach and the ratio approach to extraction the polarization. The RMS width of the difference distribution is about 0.02.

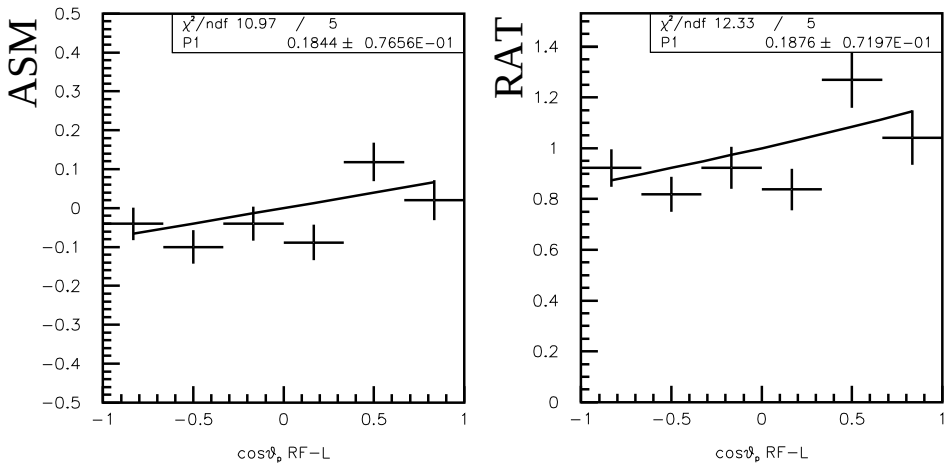

Figure 1: Comparison of polarization fits with the asymmetry and ratio extraction methods for the 4 GeV data summed over all Q^2 and all $d\Omega^*_K$ for the W bin from 1.6 to 1.7 GeV.

There is also a systematic uncertainty contribution that arises due to binning choices made during the data sorting. This results from the somewhat arbitrary choice made for the $\cos\theta^*_K$ bin size. Nominally the data was sorted into six bins in the rest frame proton angle. A comparison of these results with the extraction from a sort with six and eight bins in this variable yielded an average polarization difference of 0.02. This value has been assigned to this effect for all E1C data sets. A comparison of the nominal six bin sort vs. the eight bin sort is shown in Fig. 4. The difference in the polarization results is effectively due to the fitting algorithm employed in which the centroids of the $\cos\theta_p^{RF}$ bins are assigned to the center of the bin. When the number of bins are reduced, the fit results are more sensitive to the bin content. Fig. 3(right) shows the distribution of the polarization differences between

the nominal 6 bin sort and the 8 bin sort. The RMS width of the difference distribution is about 0.02.

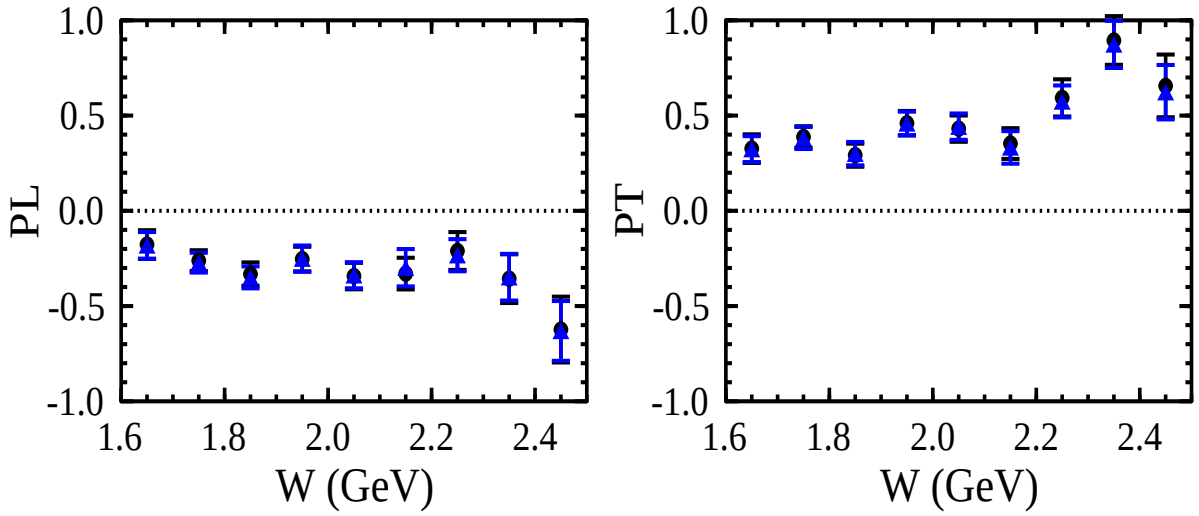

Figure 2: Comparison of the polarization fit results for P'_L and P'_T for the 4 GeV data summed over all Q^2 and $d\Omega^*_K$ for the nominal asymmetry approach (black points) and the ratio approach (blue points).

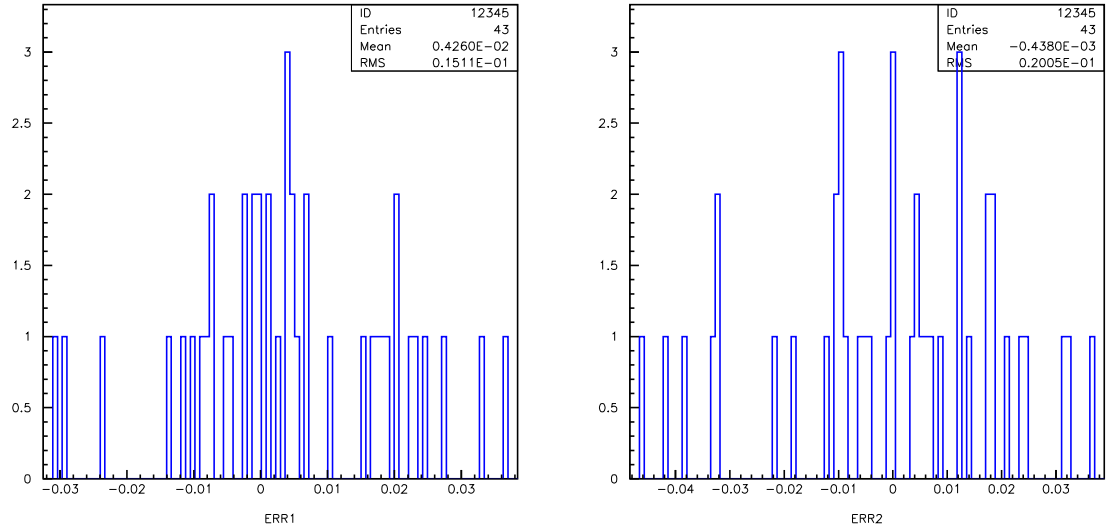

Figure 3: Distribution of the polarization difference between : (left) the nominal asymmetry approach and the ratio approach and (right) the nominal 6 bin sort and the 8 bin sort. The data points considered here are only those 4 GeV points that have been integrated over all Q^2. The distributions for the 2.567 GeV data is very comparable.

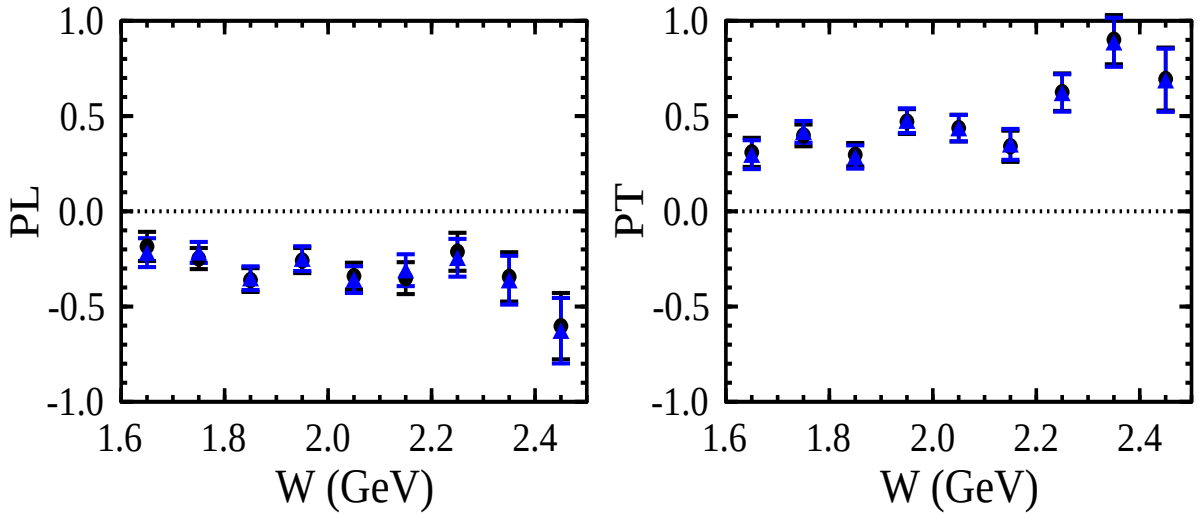

Figure 4: Comparison of the polarization fit results for P'_L and P'_T for the 4 GeV data summed over all Q^2 and $d\Omega^*_K$ for the nominal 6 bin sort (black points) and the 8 bin sort (blue points).

3 Beam Related Factors

There are two contributions to the systematic uncertainty accounting from uncertainties associated with the electron beam. The first factor is associated with the beam polarization measurement from the Møller polarimeter system. The final contribution from this effect has been discussed in other Hall B documents. The entry into our final systematic accounting from the beam polarization uncertainty includes both the statistical and systematic contributions. This has been conservatively estimated to be 1.7% for all E1C running. Note that the last two Møller measurements on 4/07/99 and 4/10/99 are not included in our considerations as they were made during portions of data collection not considered in this analysis.

As the Møller measurements were performed every 3 - 5 days during the E1C experiment, a technique to monitor the beam polarization with a finer time granularity was required. For this purpose we measured the $\langle \sin\Phi \rangle$ moment for the $K^+\Lambda$ final state on a run-by-run basis. This moment is directly proportional to the beam asymmetry term $A_{LT'}$. Ultimately, to improve the statistical precision, groups of 3 to 5 runs were added together for this analysis.

The $\langle \sin\Phi \rangle$ moment was measured using the definitions:

$$\langle \sin\Phi \rangle = \langle \sin\Phi \rangle^+ - \langle \sin\Phi \rangle^- \tag{6}$$

$$\langle \sin\Phi \rangle^\pm = \frac{1}{P_b N^\pm} \sum_{i=1}^{N^\pm} \sin(\phi)_i, \tag{7}$$

where P_b is the average electron beam polarization and N^+ and N^- refer to the number of $K^+\Lambda$ events from the positive and negative helicity states of the beam.

The $\langle \sin\Phi \rangle^\pm$ moment from each helicity state is related to structure functions and the CLAS acceptance function $A(\Phi)$ as follows:

$$\langle \sin\Phi \rangle^{+} \propto \int_0^{2\pi} \sigma_0 A(\Phi) \sin\Phi d\Phi + C \int_0^{2\pi} \sigma_{LT'} A(\Phi) \sin^2\Phi d\Phi \tag{8}$$

$$\langle \sin\Phi \rangle^{-} \propto \int_0^{2\pi} \sigma_0 A(\Phi) \sin\Phi d\Phi - C \int_0^{2\pi} \sigma_{LT'} A(\Phi) \sin^2\Phi d\Phi, \tag{9}$$

where σ_0 is given by:

$$\sigma_0 = K_f \left[R_T^{00} + \epsilon_L R_L^{00} + \sqrt{2\epsilon_L(1+\epsilon)} R_{LT}^{00} \cos\Phi + \epsilon R_{TT}^{00} \cos 2\Phi \right], \tag{10}$$

and $C = \sqrt{2\epsilon_L(1-\epsilon)} \sin\theta_K^*$. Therefore, by taking a difference of the $\langle \sin\Phi \rangle^{\pm}$ moments from the two helicity states, the helicity-independent term will be canceled out and the helicity-dependent term will survive.

Fig. 5 shows the moment analysis vs. run number for the E1C data studied in this experiment. For most runs the beam polarization was stable within statistical errors. Note the difference in signs for the moment difference between the 2.567 GeV and 4 GeV data is due to the difference in helicity convention between the two data sets.

The second beam related effect that contributes to the overall systematic uncertainty is the beam charge asymmetry that results from a systematic difference in the electron beam intensity for the two different beam helicity states. One explanation for this false asymmetry is related to the presence of broken sequences of helicity states. The helicity pattern of the electron beam is, in fact, formed by pairs of electron buckets with opposite helicity, whose order is chosen in a pseudo-random way. The helicity flip rate during the E1C run period was set mainly to 30 Hz (although it was set for short periods to 1 Hz to accommodate the priority Hall). During the acquisition process, the sequence can be interrupted by the DAQ due to dead time problems, effectively providing unpaired helicity states. Another possible explanation for a beam charge asymmetry can arise if the DAQ live times for the two beam helicity states are different. From studies of the E1C data set, no detectable difference between the live times was found.

The account for the charge asymmetry, one should measure the accumulated charge for each helicity state separately and correct for this false asymmetry. Ideally we would want to read the Faraday cup synchronously with the helicity flip and put the accumulated charge value into the data stream. However for the E1C running period the Faraday cup electronics were too slow to be able to perform the integration with the 30 Hz flip rate. In order to determine the magnitude of the beam charge asymmetry for the E1C data set, elastic *ep* scattering was analyzed [3]. As this reaction has no asymmetry, it serves as an excellent monitor of the beam charge asymmetry.

Table 2 shows the measured beam charge asymmetry for the different running conditions. The average value of this false asymmetry over all conditions is 0.03%. This level of the beam charge asymmetry affects the extracted polarization at the 0.01% level. In the current analysis, no correction is applied, and the contribution to our systematic accounting is assumed to be 0.01%.

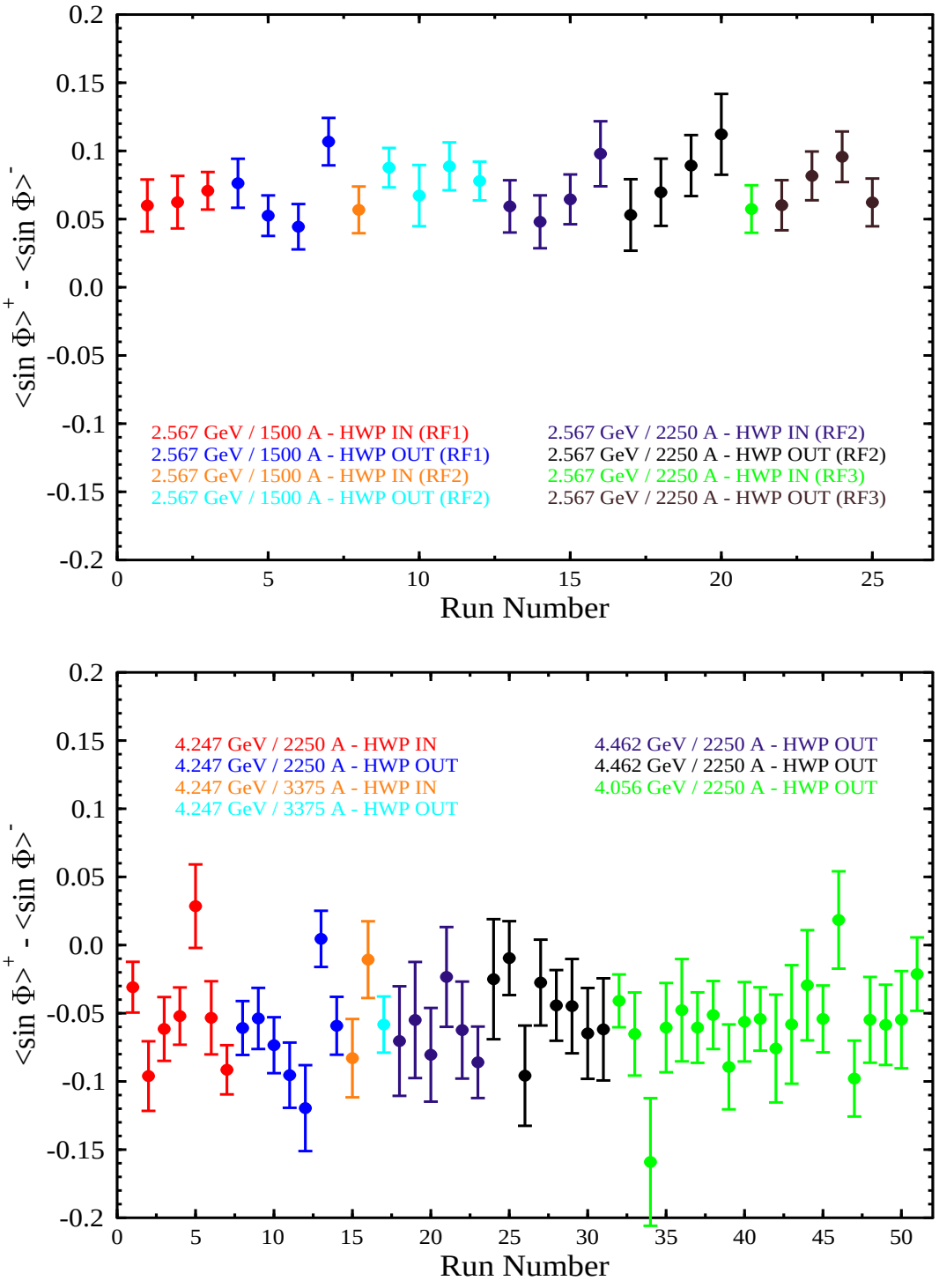

Figure 5: Results of $\sin\Phi$ moment analysis to study the beam polarization stability through the $\sigma_{LT'}$ structure function for the $K^+\Lambda$ final state in the E1C data.

Energy (GeV) / Torus (A)	Asymmetry	Stat. Uncertainty
2.567 GeV/1500 A	0.433E-03	0.178E-03
2.567 GeV/2250 A	0.113E-03	0.249E-03
4.247 GeV/2250 A	0.199E-02	0.522E-03
4.247 GeV/3375 A	0.296E-02	0.129E-02
4.462 GeV/3375 A	-0.340E-02	0.957E-03

Table 2: Beam charge asymmetries for the different running conditions of the E1C data set.

4 Acceptance Function

There are several factors that go into our final systematic uncertainty accounting associated with the form of the acceptance correction employed and with the specific choices made to implement this correction. These choices include the specific form of the fiducial cuts employed to define the azimuthal extent of the acceptance as a function of polar angle and the minimum acceptance cut off. Each of these contributing effects is discussed below.

A lengthy and detailed comparison between the different acceptance function models has been carried out for this analysis. The results are fully discussed in Ref. [4]. The different approaches are a geometrical acceptance calculation and a GSIM GEANT Monte Carlo approach. In this work the GSIM acceptance function has been employed for the 4 GeV analysis and the geometrical model has been employed for the 2.567 GeV analysis. Both models have very similar qualitative predictions for the acceptance function of CLAS, but there are clear differences in their detailed functional forms. However the beauty of the asymmetry approach employed for this analysis is that the results are relatively insensitive to the choice of the form of the acceptance correction.

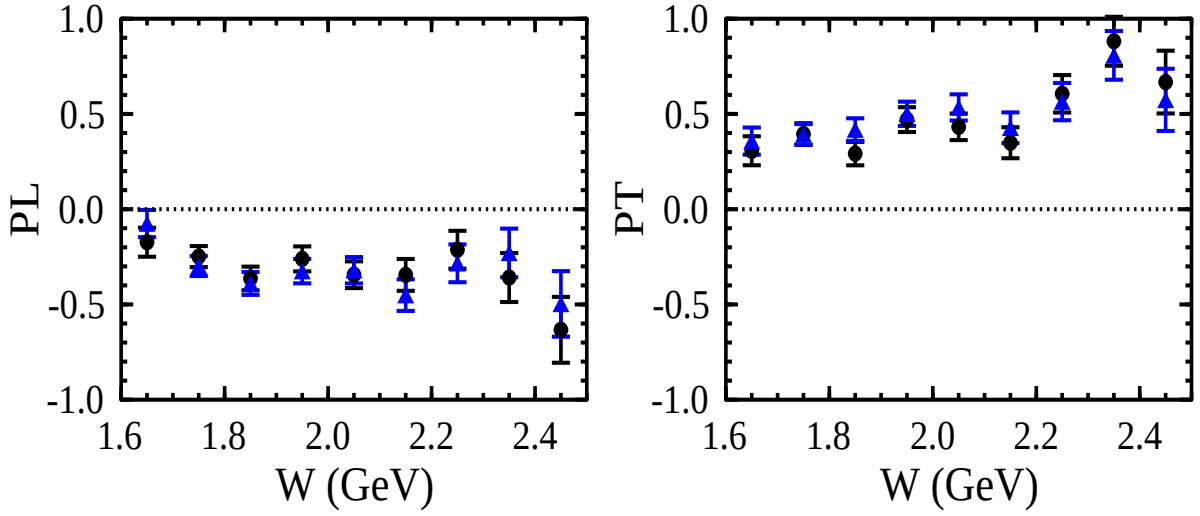

Figure 6: Comparison of the polarization fit results for P'_L and P'_T for the 4 GeV data summed over all Q^2 and $d\Omega^*_K$ for the nominal data sort with the GSIM acceptance correction (black points) and the geometrical model acceptance correction (blue points).

The first contribution to the systematic uncertainty for this analysis comes from a detailed comparison of the extracted polarization employing the GSIM acceptance function and the geometrical model acceptance. The average polarization difference employing the same set of fiducial cuts in each analysis is 0.07, which is the error assigned in our accounting. A comparison is included in Fig. 6. Note also that a comparison of the extracted polarization with no acceptance corrected applied, but with the nominal fiducial cuts in place, is also fully in accord with this error assignment as shown in Fig. 7. This uncertainty contribution has been applied to all E1C data set analyses. Fig. 8 shows the distribution of the polarization differences between the GSIM acceptance function and the geometrical acceptance model. The RMS width of the difference distribution is about 0.08.

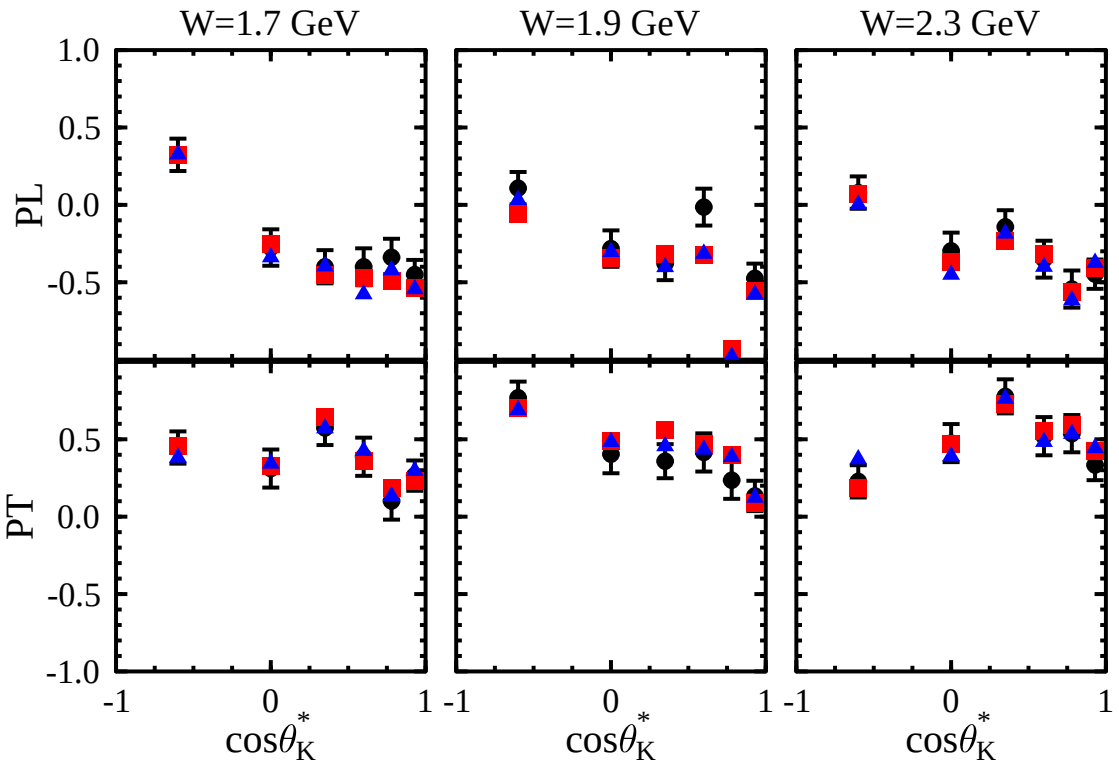

Figure 7: Comparison of the polarization fit results for P'_L and P'_T for the 4 GeV data summed over all Q^2 and Φ for three different W bins as a function of $\cos\theta^*_K$. The blue points are for the nominal data sort with the GSIM acceptance correction (black circles), the geometrical model acceptance correction (blue triangles), and no acceptance correction (red squares).

The second contribution to the systematic uncertainty associated with the acceptance function relates to the detailed form of the fiducial cuts employed to define the azimuthal acceptance for electrons and hadrons. For this comparison three sets of fiducial cuts were defined in the analysis. A loose cut (the nominal cut) was designed to just define the azimuthal acceptance edge of CLAS as a function of momentum, a medium cut was designed to be 2-3° tighter than the loose cut, and finally, a tight cut was designed to be 4-6° tighter than the loose cut. In terms of statistics, the loose fiducial cuts remove ∼8% of our final hyperon statistics after all other cuts have been made, while the medium and tight cuts

remove ∼15% and 35% of the final hyperon statistics, respectively.

The average polarization difference between the nominal loose cuts and the medium cuts was 0.03 and this was the uncertainty assigned to the fiducial cut choice. The numbers for the tight cut comparison were less favorable due to the sizeable reduction in statistics of that data set. However, Fig. 9 shows the comparison of the extracted polarization between the loose and tight cuts. Fig. 10 shows the distribution of the polarization differences between the data subject to the nominal loose fiducial cut and no fiducial cut. The RMS width of the difference distribution is about 0.05.

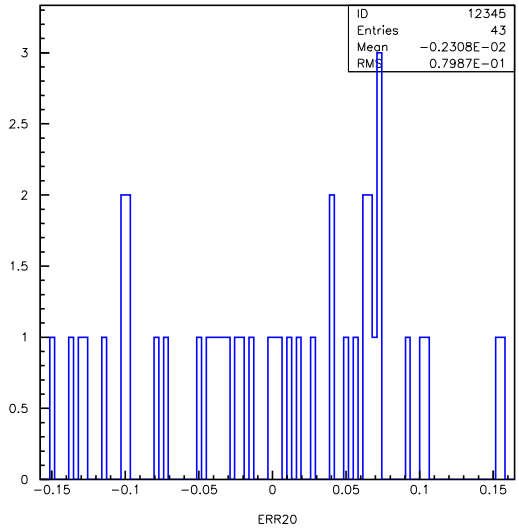

Figure 8: Distribution of the polarization difference between the polarization data corrected with the GSIM acceptance function and the geometrical acceptance function.

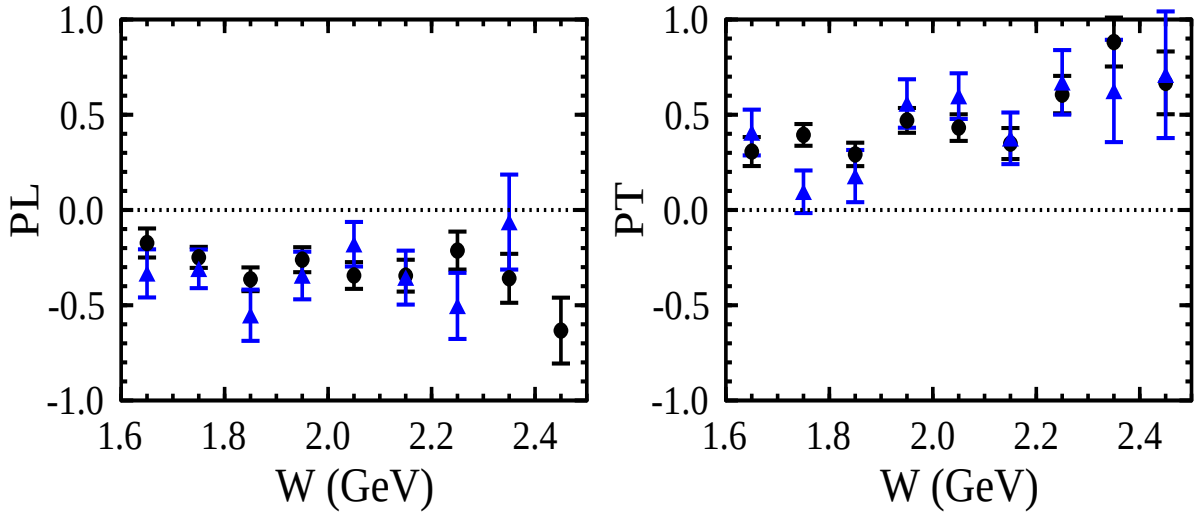

Figure 9: Comparison of the polarization fit results for P'_L and P'_T for the 4 GeV data summed over all Q^2 and $d\Omega^*_K$ for the nominal data sort with the loose fiducial cuts in place for the electrons and hadrons (black points) and with the tight fiducial cuts (blue points).

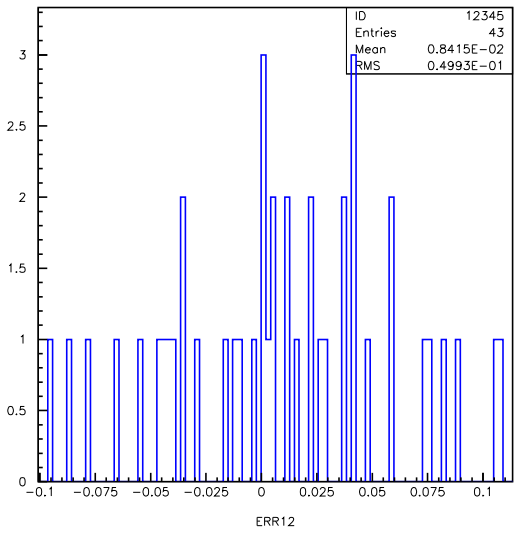

Figure 10: Distribution of the polarization difference between the polarization data subject to the nominal loose fiducial cut and no fiducial cut.

The last systematic contribution due to the acceptance function regards the specific value of the minimum acceptance cut off used in the analysis. This minimum acceptance cut off translates into a maximum acceptance weight cut off. In this analysis different maximum weight cut off values were used for the 2.567 GeV and 4 GeV analysis due to the different acceptance models employed, although the final contribution to the systematic uncertainty came out to be the same. For the 4 GeV GSIM acceptance function, the largest statistical uncertainties for the computed acceptance were associated with the bins with the smallest acceptances, and hence, the largest weights. We ultimately decided to set the acceptance cut off to include only those bins with less than a 20% statistical uncertainty on the acceptance function. The minimum acceptance cut off was set at 1% for the $e'K^+p$ final state. This removed roughly 2% of the events. For the geometrical model, the minimum acceptance cut off was set at 2% to remove roughly the same fraction of events.

The average polarization difference for the 4 GeV data was computed to be 0.045 when increasing the maximum acceptance weight cut off by a factor of two. The systematic uncertainty assigned to the weight cut off effect was 0.023, or one half this value, due to the sizeable statistical uncertainties in the acceptance function for these low acceptances. The value for the polarization difference of 0.023 is also fully consistent with the average polarization difference found in the 2.567 GeV data set employing the geometrical model. Fig. 11 shows the comparison of the extracted polarization between the nominal and lowered acceptance cut offs. Fig. 12 shows the distribution of the polarization differences between the data with the nominal 1% minimum acceptance cut off and the 0.5% minimum acceptance cut off in place. The RMS width of the difference distribution is about 0.05.

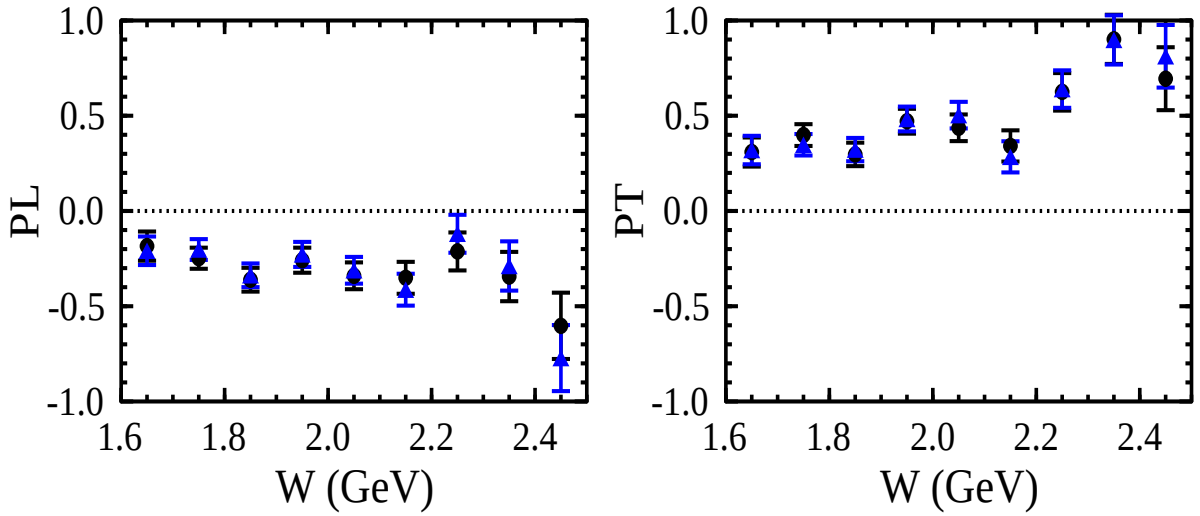

Figure 11: Comparison of the polarization fit results for P'_L and P'_T for the 4 GeV data summed over all Q^2 and $d\Omega^*_K$ for the nominal data sort with the 1% minimum acceptance cut off in place (black points) and with a 0.5% minimum acceptance cut off (blue points).

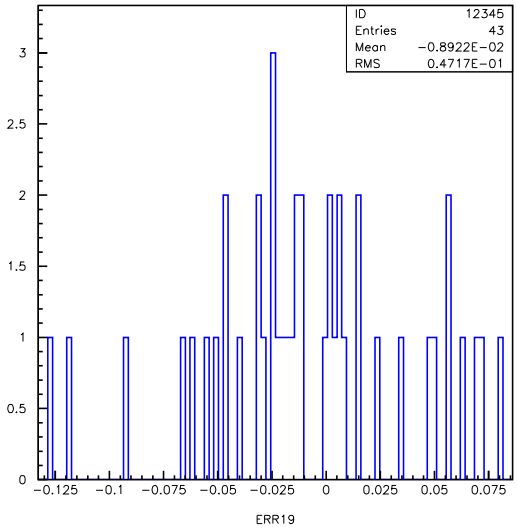

Figure 12: Distribution of the polarization difference between the polarization data with the nominal 1% minimum acceptance cut off and the 0.5% minimum acceptance cut off in place.

5 Background Contributions

Our analysis of the backgrounds found no measurable level of Σ^0 contamination within our final $K^+\Lambda$ event sample. However, there is a few percent contamination of π^+ misidentification events that remain before the background subtraction. To estimate the systematic uncertainty associated with our subtraction technique we have compared the average polarization difference between our nominal background-subtracted results and the results from a sort with very tight fiducial cuts on the π^- missing mass vs. hyperon missing mass correlation. The box cut defined in Fig. 13 was designed to remove the vast majority of the pion

background. The average polarization difference was measured to be 0.02. Our systematic uncertainty was assigned conservatively to be one half this value, or 0.01, as background remains under the Λ locus that the defined cut cannot remove.

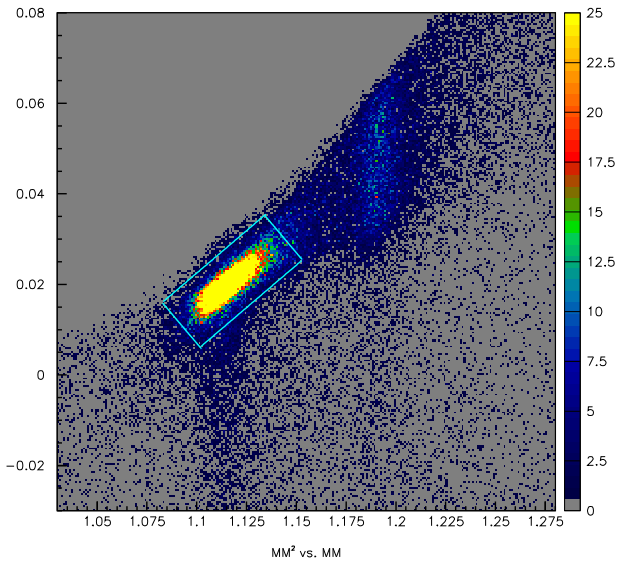

Figure 13: Plot of $e'K^+p$ missing mass squared (GeV^2) vs. $e'K^+$ missing mass highlighting the tight cut defined to estimate the systematic error associated with the pion background subtraction technique.

6 Final Systematic Uncertainty Accounting

Our final systematic uncertainty accounting is included in Table 3 listing all of the sources discussed above. The final value in the Table adds all the individual contributions in quadrature.

Category	Contribution	Systematic Uncertainty
Polarization Extraction	Functional Form	0.013
	Bin Size	0.02
Beam Related Factors	Beam Polarization	1.7%
	Beam Charge Asymmetry	0.01%
Acceptance Function	Functional Form	0.07
	Fiducial Cut Form	0.03
	Acceptance Cut Off	0.023
Background Contributions	Pion Contamination	0.01
$\langle$ **Total Systematic Error** $\rangle$		0.084

Table 3: Summary Table of the results obtained in the systematic studies.

7 Other Systematic Studies

In the course of the polarization analysis, many other studies of systematic effects were carried out. This allowed us to gain further confidence in both the quality of our data sets, as well as the soundness of our analysis approach. Some of these studies are included in this section for completeness.

1). In order to study the response of the CLAS detector itself, the analysis was studied comparing the polarization results for the electron in each of the six CLAS sectors. A sector-by-sector analysis is of poor statistical quality, but clearly shows that the results agree within error bars. Fig. 14 shows a comparison of the results with the electron in sectors $1 \rightarrow 3$ vs. sectors $4 \rightarrow 6$. The results are consistent independent of the choice of the set of sectors highlighting that the physics results are independent of ϕ_e^{lab}.

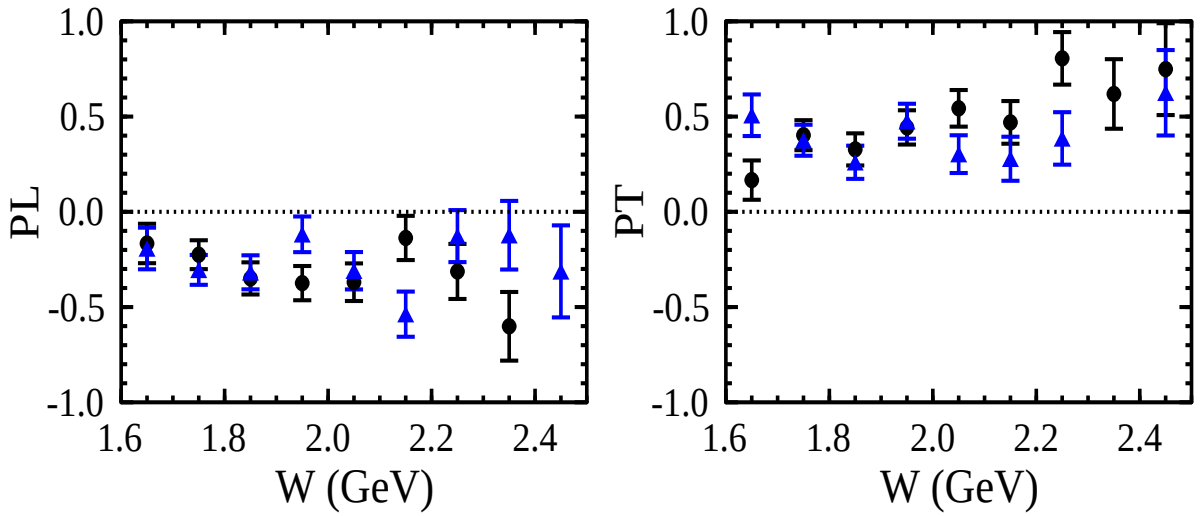

Figure 14: Comparison of the polarization fit results for P'_L and P'_T for the 4 GeV data summed over all Q^2 and $d\Omega^*_K$ for the electron in sectors $1 \rightarrow 3$ (black points) vs. the electron in sectors $4 \rightarrow 6$ (blue points).

2). The analysis results have been studied in detail as a function of the cuts employed on the hyperon mass spectrum, as well as the π^- mass spectrum to identify the Λ hyperons and remove the Σ^0 background. The effect of these cuts and their influence on the extracted polarization results is accounted for in the systematic uncertainty assigned to the background subtraction procedure.

3). The polarization results have also been compared separately for the two positions of the half-wave plate. This analysis, assuming the same magnitude of the beam polarization for each setting, is shown in Fig. 15. The systematic uncertainty associated with the beam polarization dependence on the half-wave plate position is accounted for within the error quoted for the beam polarization systematic.

4). In this analysis a minimum cut-off momentum for the kaons of 300 MeV/c is included. The effect of changing this value to 100 MeV/c or 500 MeV/c has essentially no effect on

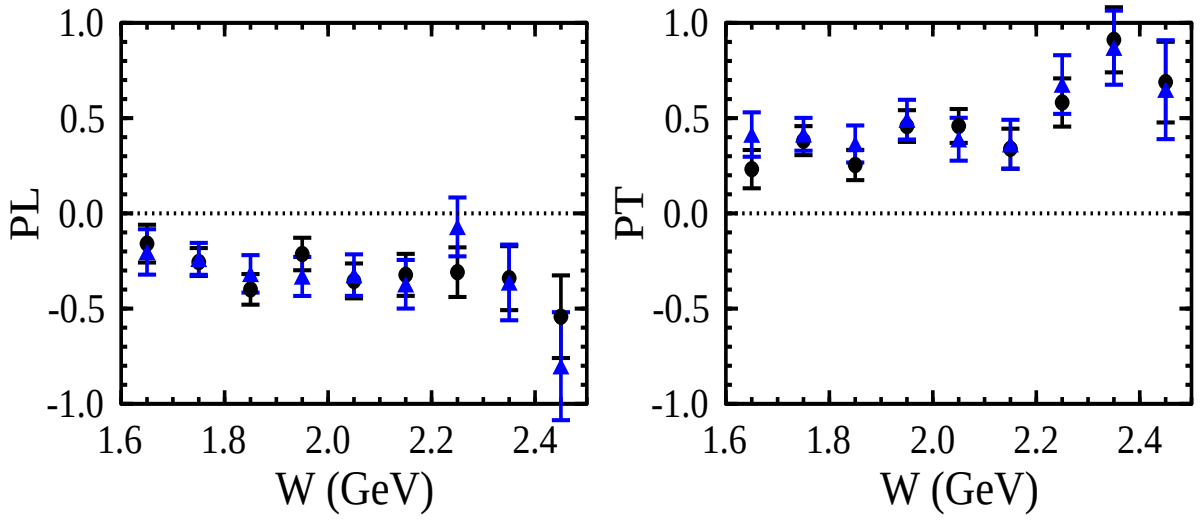

Figure 15: Comparison of the polarization fit results for P'_L and P'_T for the 4 GeV data summed over all Q^2 and $d\Omega^*_K$ for the setting with the half-wave plate in (black points) and out (blue points).

the extracted polarization values.

5). In this analysis the polarization results for different CLAS torus settings are combined mainly to increase the statistical precision of the data. Comparison of the 40% and 60% field settings at 2.567 GeV and the 60% and 90% field settings at 4 GeV are shown in Fig. 16. Good agreement is found between both sets of data giving us confidence in the data combination.

6). A third technique to extract the hyperon polarization has been explored. This technique serves as an important cross check of our results. It is not included in the discussion in Section 2 as it is slightly more sensitive to the detailed form of the acceptance correction function. Each polarization component can also be written as:

$$P'_\Lambda = \frac{2}{\alpha P_b} \frac{\sigma_F - \sigma_B}{\sigma_F + \sigma_B}, \tag{11}$$

where σ_F and σ_B represent the acceptance-corrected decay proton yields going forward and backward in the hyperon decay frame relative to θ_p^{RF}=90°.

This analysis yields an average polarization difference compared to the nominal results with the asymmetry method of 0.05. The results of the polarization comparison are shown in Fig. 17.

7). Another way to gain confidence in the analysis approach is to extract the normal transferred polarization components P'_n, P'_y, and $P'_{y''}$, each of which should vanish when integrated over all Φ. The results of the analysis, included in Fig. 18 from the 2.567 GeV data analysis and Fig. 19 from the 4 GeV analysis, indicate that these components are consistent with zero.

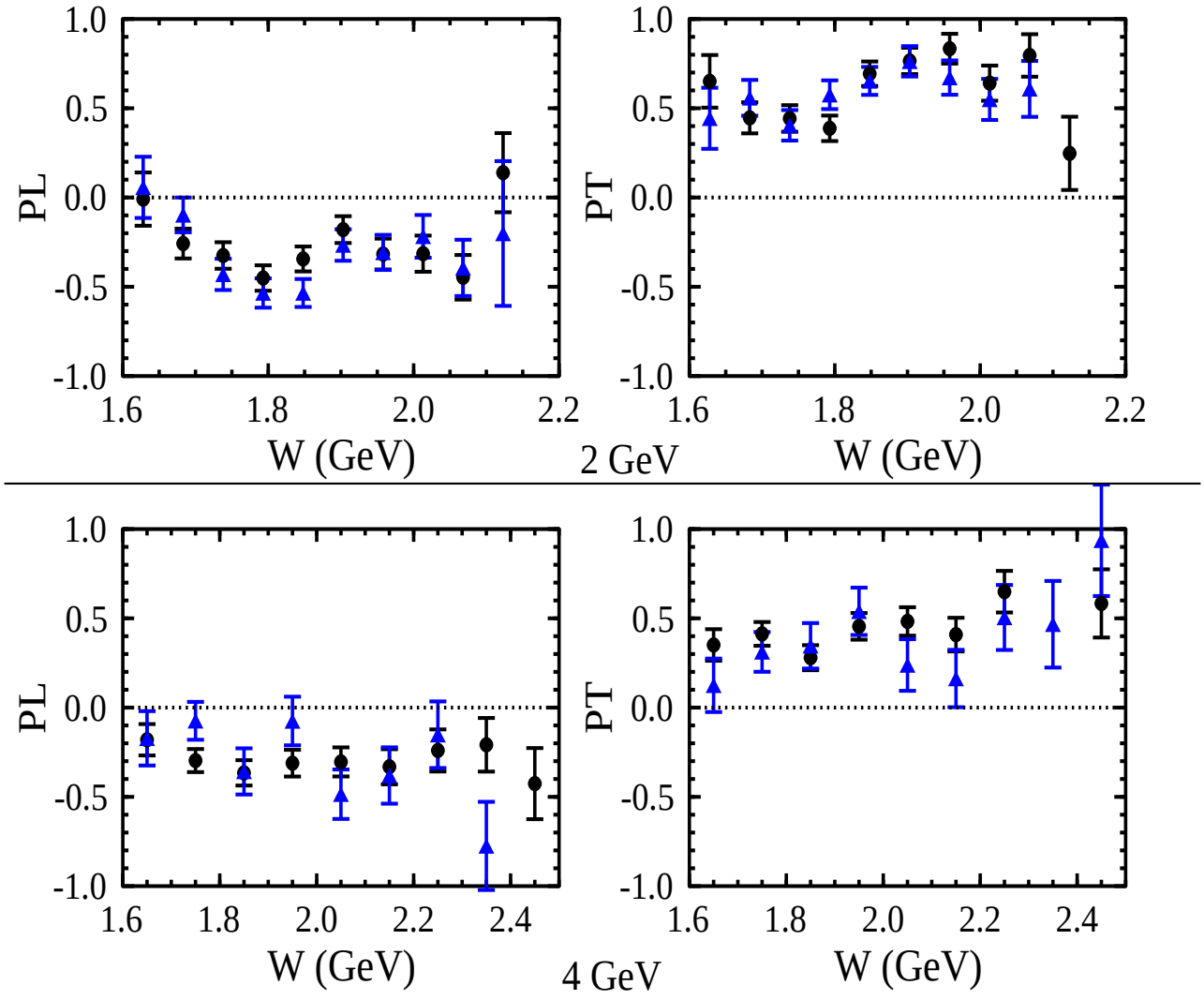

Figure 16: Comparison of the polarization fit results for P'_L and P'_T for the 2.567 GeV data (upper plots) at 40% field (black points) and 60% field (blue points), and for the 4 GeV data (lower plots) at 60% field (black points) and 90% field (blue points).

8). The last effect to highlight is a comparison of the polarization extracted separately for each beam helicity state. This extraction can be accomplished using the forward/backward ratio method alluded to above. This analysis is very sensitive to the specific functional form of the CLAS acceptance, the event generator employed, and the statistical precision of the acceptance. Each of the effects are essentially eliminated with either the asymmetry or ratio approaches to the analysis. More details regarding the limitations of the acceptance function are contained in Ref. [4].

The comparison of the polarization extracted for each beam helicity state is shown in Fig. 20. There are clear differences between the helicity states. This is certainly not too surprising given the known limitations in the acceptance calculation. However, the comparison is provided for completeness of the discussion.

As a follow up study to provide further understanding and insight into this particular issue, a program was written to generate data with one acceptance function and to reconstruct

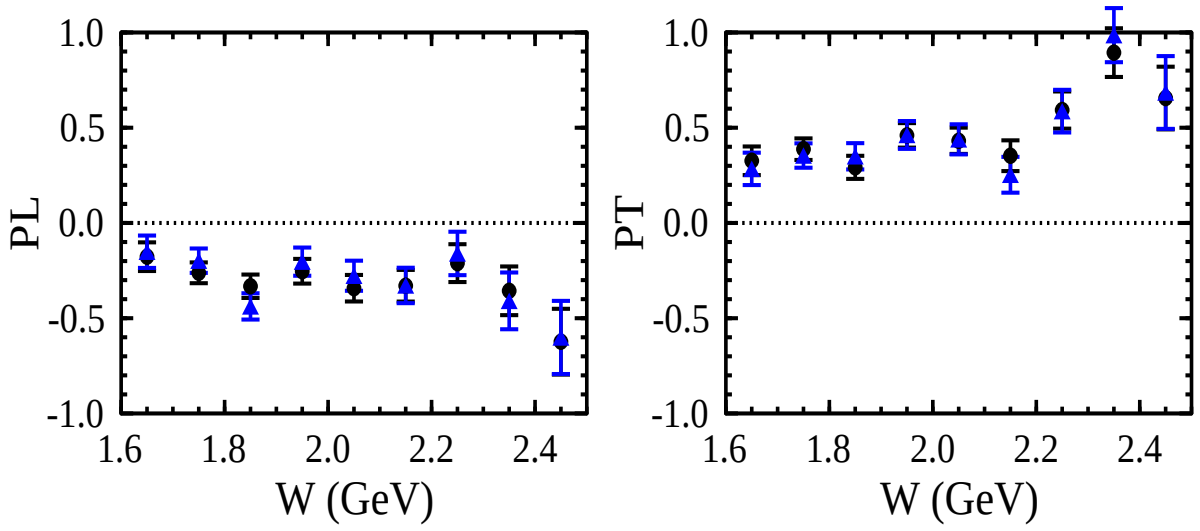

Figure 17: Comparison of the polarization fit results for P'_L and P'_T for the 4 GeV data summed over all Q^2 and $d\Omega^*_K$ for the polarization extracted with the nominal asymmetry method (black points) and with the forward/backward ratio method (blue points).

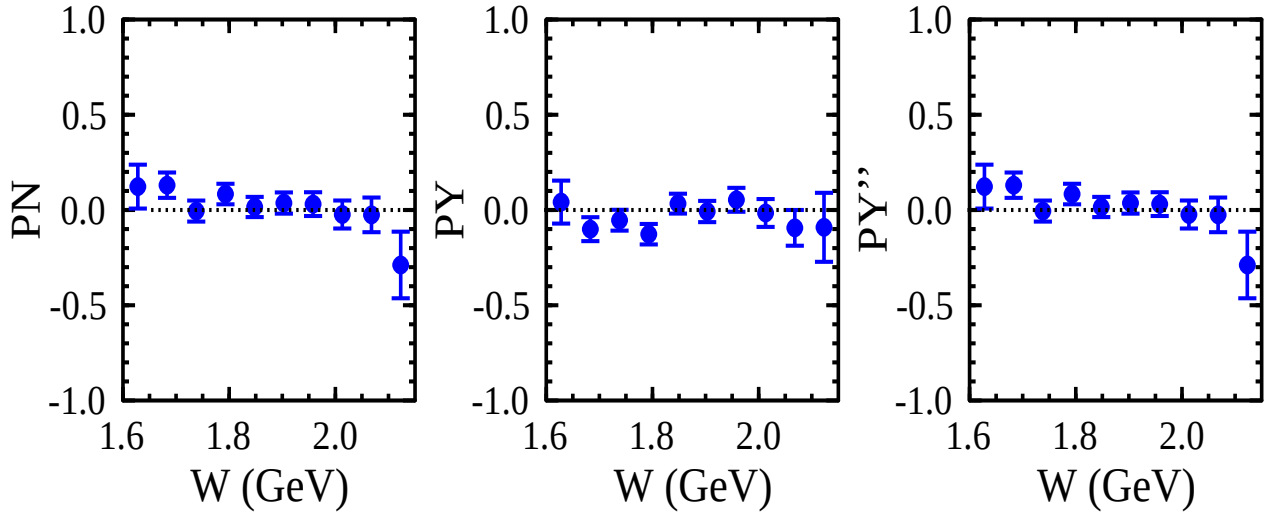

Figure 18: Comparison of the polarization fit results for P'_n, P'_y, and P''_y for the 2.567 GeV data summed over all Q^2 and $d\Omega^*_K$. These components are expected to vanish for integration over all Φ. Note that the components P_n and P''_y have the same definition.

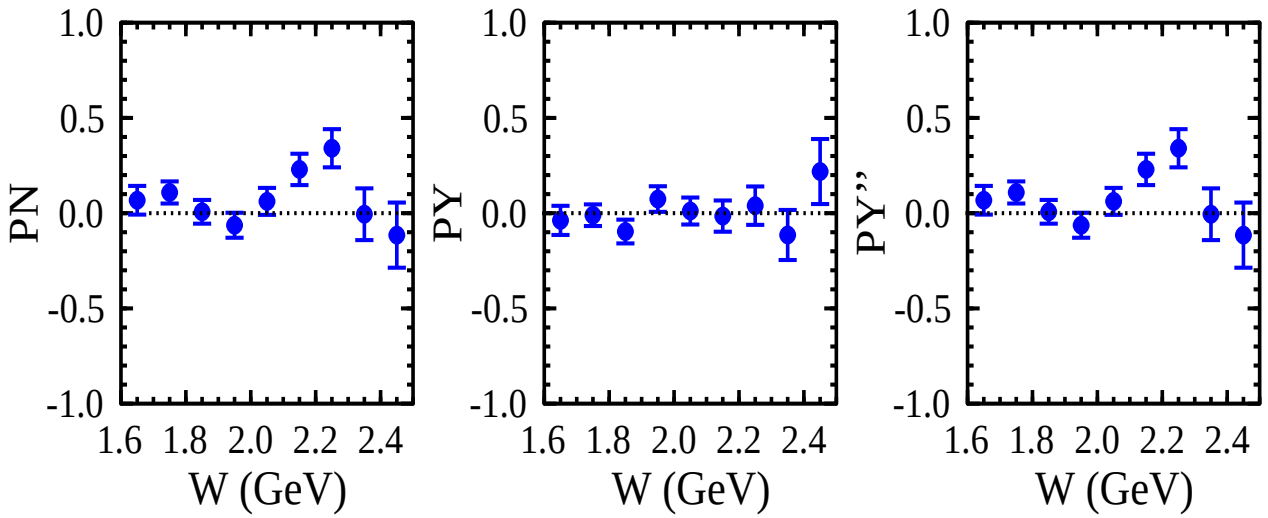

Figure 19: Comparison of the polarization fit results for P'_n, P'_y, and P''_y for the 4 GeV data summed over all Q^2 and $d\Omega^*_K$. These components are expected to vanish for integration over all Φ. Note that the components P_n and P''_y have the same definition.

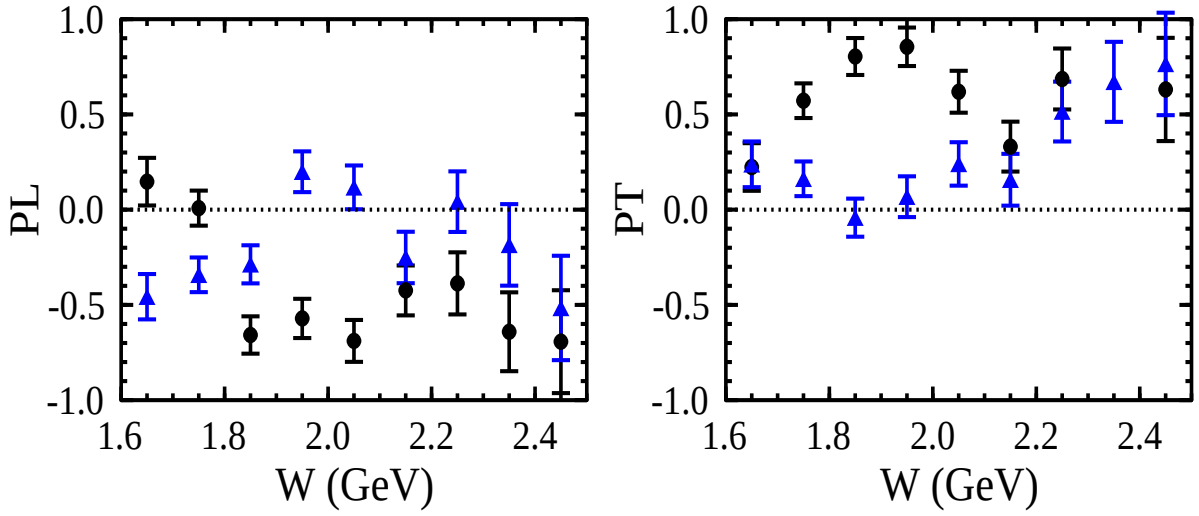

Figure 20: Comparison of the polarization fit results for P'_L and P'_T for the 4 GeV data summed over all Q^2 and $d\Omega^*_K$ for the positive helicity state of the electron beam (black points) and the negative helicity state (blue points).

it with another. This is exactly what would occur if there were problems with the acceptance function used to correct the data. The study was performed with the acceptance function depending only on $\cos\theta_p^{RF}$, with functional forms consistent with our expectations from the geometrical acceptance model and GSIM (see plots in Ref. [4]). The acceptance functions considered are shown in Fig. 21 and were assumed to be independent of beam helicity. The functions considered in Fig. 21(a-c) are linear with $\cos\theta_p^{RF}$, similar to what has been seen in our Monte Carlo studies. The non-linear acceptance function shown in Fig. 21d has been included to show that the results of the study are not sensitive to the detailed form of the acceptance function.

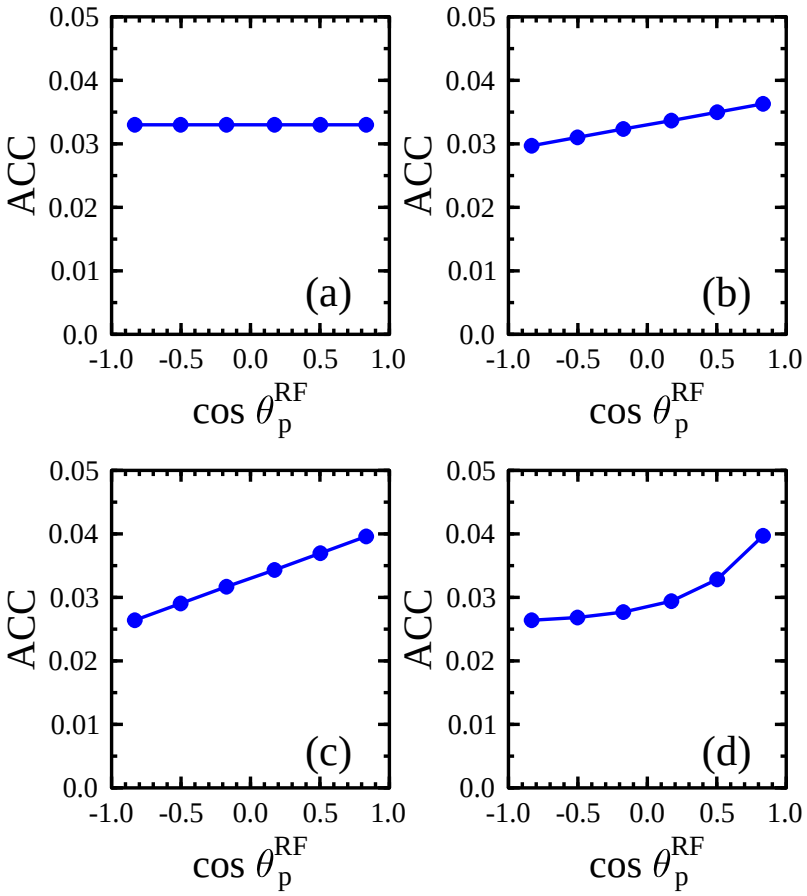

Figure 21: The functional forms for the acceptance function vs. $\cos\theta_p^{RF}$ employed in the study of the sensitivity of the helicity-separated polarization results to the acceptance.

The results of the study are shown in Figs. 22 and 23. Here the data was generated with a flat acceptance versus $\cos\theta_p^{RF}$ (Fig. 21a) and reconstructed with each of the different acceptance functions using both the asymmetry approach and extracting the polarization separately for each beam helicity state. Included in Figs. 22 and 23 are the values extracted from the polarization analysis in this study. The beam polarization employed for the study was 70% and the Λ polarization was 45%, both typical values for this analysis. Fig. 22 shows the acceptance-corrected yields from this study separately for each beam helicity state. In the left plot the data is reconstructed with the acceptance function of Fig. 21a, in the middle plot it is reconstructed with that in Fig. 21b, and in the right plot it is reconstructed with

that in Fig. 21c. When the acceptance function used to extract the helicity-separated results is not an accurate representation of the true acceptance function, the helicity-separated polarization measurements (here labeled $P+$ and $P-$) have sizeable errors. However, as long as the acceptance function is the same for both helicity states, the extracted polarization using the asymmetry approach (the value shown in Fig. 22 between the upper row and lower row of plots) is accurate.

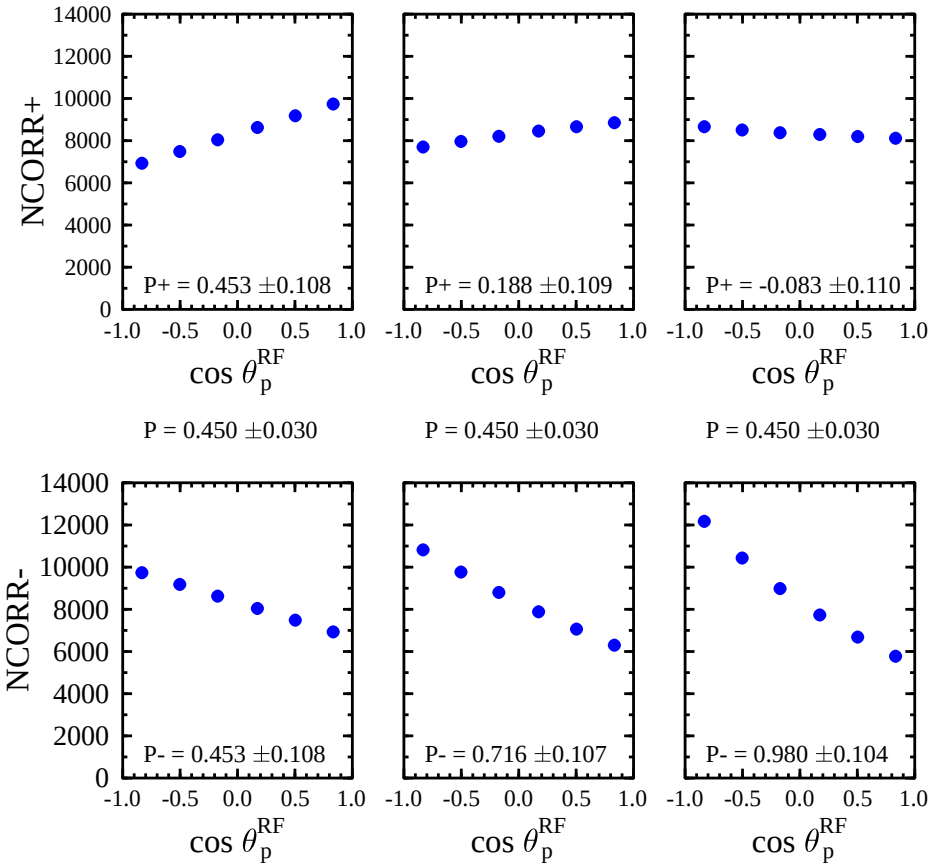

Figure 22: Acceptance-corrected yields for each beam helicity state. The data was generated with the acceptance function of Fig. 21a (flat) and then reconstructed with each of the linear functions in Fig. 21. The left column used Fig. 21a, the middle column Fig. 21b, and the right column used Fig. 21c.

The study clearly demonstrates the sensitivity of the helicity-separated extraction to the detailed form of the acceptance function. The extracted polarization using the asymmetry approach is completely insensitive to the acceptance in these studies. Note that the slope of the CLAS acceptance with $\cos\theta_p^{RF}$ has been found to be W dependent. It is this effect that is primarily responsible for the variation in the spread of the helicity-separated results in the CLAS data shown in Fig. 20.

The conclusions drawn above are insensitive to the functional form of the acceptance function. The results of the polarization extraction for the helicity-separated results and for the asymmetry approach are shown in Fig. 23 reconstructing the data with the non-linear acceptance function shown in Fig. 21d.

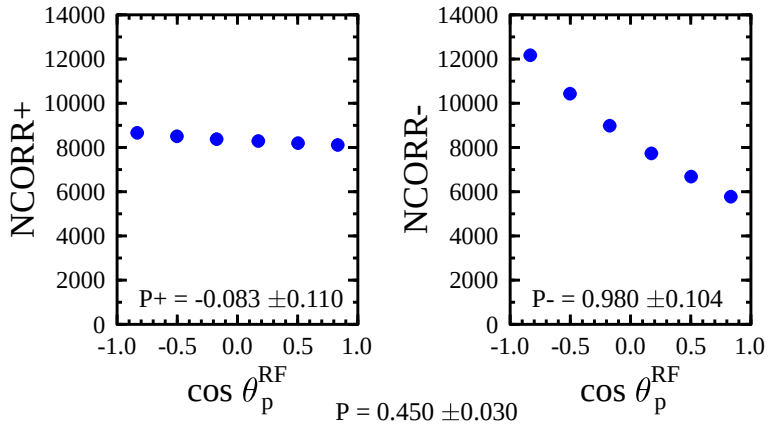

Figure 23: Acceptance-corrected yields for each beam helicity state. The data was generated with the acceptance function of Fig. 21a (flat) and then reconstructed with the non-linear function in Fig. 21d.

References

[1] D.S. Carman, K. Joo, B.A.Raue *et al.*, JLab Experiment E99-006.

[2] D.S. Carman and B.A. Raue, "Hyperon Electroproduction at CLAS: $p(\vec{e}, e'K^+)\vec{\Lambda}$", E99-006 Analysis Document, unpublished, (2002).

[3] L. Kramer *et al.*, "Analysis of e1c Beam Charge Asymmetries", CLAS-Note 2001-012.

[4] M.U. Mozer and D.S. Carman, "Comparison of GSIM Monte Carlo and Geometric Acceptance Functions for CLAS", CLAS-Note 02-005, (2002).